Ceramics International 46 (2020) 21248–21255

Contents lists available at ScienceDirect

Ceramics International

journal homepage: www.elsevier.com/locate/ceramint

Atmospheric flame vapor deposition of WO_3 thin films for hydrogen detection with enhanced sensing characteristics

M. Torabi Goodarzi, M. Ranjbar*

Department of Physics, Isfahan University of Technology, Isfahan, 8415683111, Iran

ARTICLE INFO

Keywords:
Solid-feed flame vapor deposition (SF-FVD)
WO_3
Thin films
Hydrogen sensor
FESEM

ABSTRACT

Nowadays, with the increasing demand for hydrogen, sensors that can detect low concentrations of this gas are essential for its safe use. In this paper, Pd/WO_3 film hydrogen sensors are developed using a solid-feed flame vapor deposition (SF-FVD), as an atmospheric, economical, and fast film fabrication method. The crystal structure and morphology of the samples were characterized by different means. The performance of the obtained sensors was investigated for different hydrogen concentrations (1–2500 ppm) and at different operating temperatures (100–250 °C). We attempted to determine the optimum deposition conditions, including feed and substrate to flame nozzle distances. In most of the sensing conditions, the response and recovery times were measured in the order of 20 to 30 s. The layer with a more open morphology showed sensitivity at ppb hydrogen level, good stability, and selectivity. The response behavior of the samples was explained according to the power-law in the metal oxide semiconductor (MOS) gas sensors.

1. Introduction

In recent years, hydrogen has received a great deal of attention as a renewable, clean, high-efficiency, and high-energy source of energy. However, there are several barriers to the use of this gas, such as high explosiveness at 4–75% concentration range, high leakage, and low explosion threshold energy [1–4]. Because it is an odorless, colorless, and tasteless gas, it cannot be detected by the human senses. Therefore, sensors capable of detecting low concentrations of H_2 with reliable performance are essential in the processes from hydrogen production to usage.

It is known that many metal oxide semiconductors (MOS) exhibit a noticeable change in resistivity upon reaction with H_2, thus providing a basis for sensing of this gas [5–12]. MOS sensors are of more interest because they are low cost, reliable, have a simple operating mechanism, and are well integrate-able to microelectronic devices.

Tungsten oxide films, with several orders of magnitude changes in resistance in reaction with hydrogen, is one of the most promising candidates among the MOS thin film gas sensors [4,13,14].

Several fabrication methods have been used so far for thin film WO_3 gas sensors (Table .1). Despite the deposition technique, a thin Pd layer improves the sensing characteristics dramatically [24–28]. This improvement in the performance has led to 1 ppm limit of detection at room temperature, a wide range of concentration detection and reducing the response and recovery time to a few seconds [13,14,26,29]. The cost-effective methods by which highly porous layers are obtained are preferred to achieve enhanced gas-surface adsorption.

Flame-based synthesis methods have been successfully employed in the mass-production of MOS nanostructures due to their capability in continuous operation at the atmospheric pressure with no need to vacuum facilities and extraordinarily high tunable temperatures and different configurations [30–35]. SF-FVD has the advantage of simple assembly and using the solid precursor in addition to gas and liquid precursors [36,37]. In the deposition of WO_3 with a solid-feed SF-FVD method, a flame oxidizes and evaporates a W metal mesh, wire or rod to produce W oxide vapor, which subsequently condenses on a surface to form films of distinct morphologies such as granular, nanowires and even nanotubes [38–41]. Fuel used in the synthesis of WO_x nanostructures is mainly a pre-mixed mixture of CH_4, O_2, Ar or N_2. According to the literature, significant reports in which the solid-feed SF-FVD method has been used to develop WO_3 hydrogen sensors have not yet been published, while this method has unique advantages [42–44]. It should be noted, however, that due to the high temperature of the flame, this method is usually limited to film deposition on refractory substrates such as alumina.

Very recently, we have used oxyhydrogen (derived from water splitting) flame to produce molybdenum oxide nanoparticles for

* Corresponding author.
E-mail address: ranjbar@iut.ac.ir (M. Ranjbar).

https://doi.org/10.1016/j.ceramint.2020.05.215
Received 10 May 2020; Received in revised form 17 May 2020; Accepted 19 May 2020
Available online 21 May 2020

Table 1
Comparison of fabricated sensors by different metal oxide sensing elements for the detection of H_2 gas with low concentration and high performances.

Sensor material	Fabrication method	Working temperature (°C)	Response	Limit of detection (ppm)	Response time (s)	Recovery time (s)
Single crystal Pt/WO_3 [13]	Pulsed laser deposition	25–65	100 (100 ppm)	1	1	> 10
WO_3 nanotubes with Pd catalyst [15]	Coaxial electrospinning	450	17.6 (500 ppm)	10	25	–
NiO nanostructure [16]	thermal oxidation & RF sputtering	150	119.63% (1000 ppm)	30	6	0.5
Mesoporous In_2O_3 [17]	Hydrothermal & calcination	260	18 (500 ppm)	0.01	1.7	1.5
SnO_2 nanofibers [18]	electrospinning	150	2.4 (1000 ppm)	600	21	33
Honeycombed SnO_2 [19]	Wet chemical	340	8.4 (1 ppm)	0.05	4	10
TiO_2 thin film [20]	Sol-gel	175	55% (10000 ppm)	100	2	464
CuO NW network [21]	Chemical solutions	300	340 (100 ppm)	–	60	2
CeO_2-loaded In_2O_3 hollow spheres [22]	hydrothermal	160	20.56 (50 ppm)	0.01	1	9
Pt/Pd on ZnO nanorod clusters [23]	Template assisted method, hydrothermal & PLD	100	2.5 (10000 ppm)	0.2	5	76
Pd/WO_3 nanostructured layer (this work)	SF-FVD	150	116.1 (12 ppm)	< 75 ppb	4	8

hydrogen sensing [45]. It has been found that this method works well on Mo and W metals. So in this article, we attempt to deposit tungsten oxide films on alumina and use them for hydrogen sensing. Probably one advantage of the technique presented in this paper is the simplicity of the deposition setup compared to similar flame-based methods such as spray pyrolysis [33,46]. Another significant contribution of the article is the high sensitivity of the obtained Pd/WO_3 layers to hydrogen gas at the ppb level. The role of the SF-FVD parameters is studied to fabricate hydrogen gas sensors. Investigations have promising results in comparison with other hydrogen gas sensors listed in Table .1. Results suggest that besides sustaining the optimum properties of the sensor, the solid-feed SF-FVD method can be used for mass production with low-cost, fast process and without requiring sophisticated vacuum facilities.

2. Experimental

2.1. Design and fabrication of SF-FVD

In this research, a homemade oxyhydrogen generator was designed and used as a flame source for the production and deposition of tungsten oxide vapor. This instrument uses DI water to produce steam of H_2/O_2 (2:1 ratio) with an 80 sccm flow rate. For the project purpose, the naked-eye visible length of the flame was adjusted about 5 cm. The resulting oxy-hydrogen flame has a bright color and sharp tip.

2.2. WO_3 and Pd layer deposition

Alumina sheets, with dimensions of 10 × 10 mm^2 selected as substrate. Before the WO_3 deposition, a pair of gold Inter-Digital Electrodes (IDEs) has deposited on its surface by the magnetron DC sputtering by a shadow mask in which the distance between each collecting electrodes was 200 μm. The deposition of WO_3 films was performed in a one-step process. To do this, we put a W metallic rod (purity = 99.6% and ø = 2.4 mm), and Al_2O_3 substrates were at a distance of d_r and d_s, respectively, from the nozzle tip (Fig. 1(a) and Table .2). The flame was oxidizing and evaporating the W rod surface during the deposition process. The oxide species propagate across the flame to form a film on the substrates (Fig. 1(b)). Only a 2 min total deposition time was sufficient to achieve hundreds of nanometer thicknesses, indicating the process is fast comparing with traditional deposition methods. A schematic illustration for the WO_3 sensor layer on IDE coated substrate is depicted in Fig. 1(c). A thin Pd layer (~4 nm) as an H_2 catalyst was deposited on the WO_3 films by DC magnetron sputtering system working at 100 mA and 400 V (40 W power) for 3 s. The deposition pressure was set to 6 × 10^{-5} Torr during the Pd deposition process.

2.3. Material characterization

The crystal structure of the deposited layers characterized by X-ray diffraction apparatus (Asenware AW-XDM300) at 2θ range of 10–80° in Grazing mode with incident radiation angel of 0.8°. The surface morphology and elemental analysis of tungsten oxide layers carried out by FEI QUANTA 450 FESEM. The gas sensing test was performed under static injection of predefined concentrations of H_2 gas in a homemade test chamber, with 3 min exposure time, under different temperatures (100, 150, 200 & 250°C). The desired concentrations were obtained by diluting the initial 0.5% hydrogen gas using a series of mass flow controllers. The used dilution gas was Argon, and background gas for the recovery process was ambient air. In all the tests, the relative humidity (RH) was about 30%. A circuit, as depicted in Fig. 1(d), was used to measure the electrical resistance of the sensors. It was designed for the measurement of high resistances. Resistant was recorded by an IVIUMSTAT potentiometer apparatus at current ChronoAmperometry mode with 2 V applied bias.

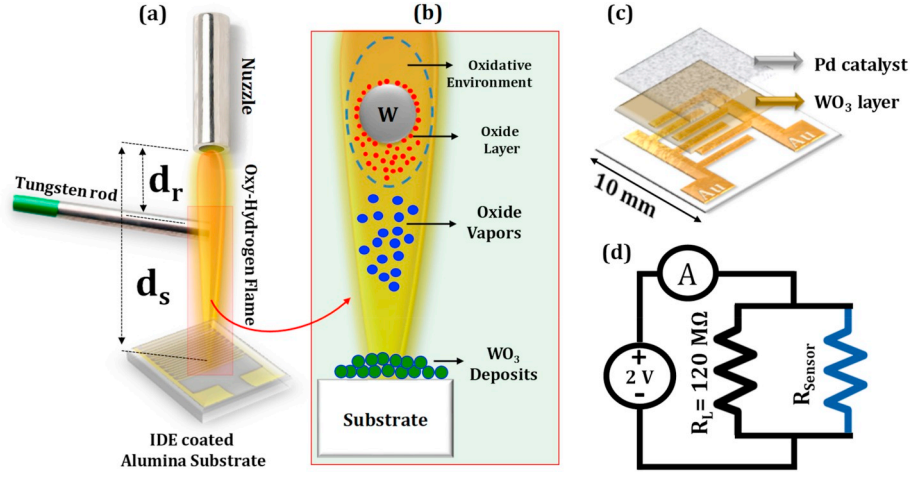

Fig. 1. Fabrication procedure of WO_3 films by SF-FVD method, (a) schematic presentation of synthesis parameters, (b) synthesis and deposition process of the tungsten oxide layer, (c) schematic illustration of IDE coated substrate and deposited WO_3 layer and (d) used circuit for the resistant measurements.

Table 2
Flame vapor deposition parameters for the fabrication of WO_3/Al_2O_3 films.

Sample name	S_1	S_2	S_3
d_r: rod-nozzle distance (mm)	10	15	15
d_s: substrate-nozzle distance (mm)	25	20	30

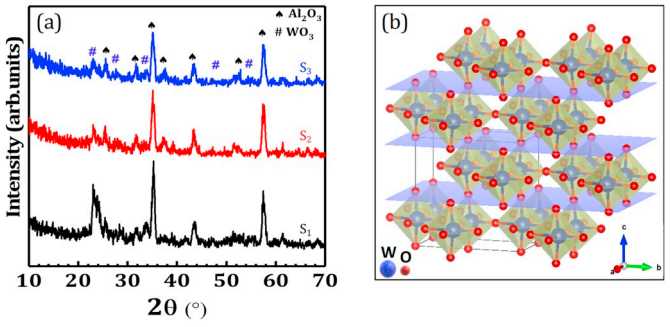

Fig. 2. (a) GIXRD patterns of WO_3/Al_2O_3 films deposited by the SF-FVD method at different conditions (see Fig. 1 and Table 2), (b) Schematic illustration of the orthorhombic WO_3 structure.

2.4. Gas sensing

The sensor response for reducing gas, R, is defined as

$$R = \frac{R_{Air} - R_{Gas}}{R_{Gas}} \quad (1)$$

where R_{Air} is the base resistance of the sensor in air, and R_{Gas} is the resistance measured in the presence of reducing gas. Response time is defined as the time required for the sensor resistance to drop by 90% of the total resistance during a reducing gas exposure, and recovery time is the time needed for the resistance change to recover by 90% during the baseline recovery process [14]. The response of the sensors was studied under different concentrations of 1, 3, 6, 12, 25, 50, 125, 250, 500 & 2500 ppm. For selectivity investigations, analyte gases were dynamically injected to the test chamber by a flow rate of 20 sccm for 60 s.

3. Results and discussions

3.1. XRD

The crystalline structure of the samples obtained from the SF-FVD method was studied using GIXRD (Fig. 2(a)). The sharp peaks observed in the patterns are related to the Al_2O_3 substrate. Other peaks confirm the formation of tungsten oxide orthorhombic structure (Card number: 00-020-1324 JCPDS) for all the SF-FVD conditions. Orthorhombic tungsten oxide is reported to have better stability in interaction with hydrogen than its other structures [47]. This structure is schematically shown in part (b), in which the corner-sharing WO_6 octahedral are deformed and tilted to form parallel plates along the *c* axis.

3.2. FESEM

Fig. 3 shows the FESEM images of the WO_3 samples. The bottom panel also shows a typical EDS elemental map of Pd/WO_3 layers, indicating the presence of W, O, and Pd elements. In all the images, the alumina substrates are clearly visible, covered with a nanostructured WO_3 layer. Sample S_1, with a shorter rod-nozzle distance, is much thicker (~600 nm) than the other two samples (~120 and 110 nm).

Besides, there is a significant difference in the microstructure of sample S_1 compared to the two other samples, which consists of flower-like WO_3 clusters that can provide a more porous body for hydrogen adsorption. The individual nanoparticles in the WO_3 clusters, shown on a typical TEM image, are about 100 nm in size. The surfaces of samples S_2 and S_3 have larger grains, which appear to be more tightly clamped together. Therefore, in our SF-FVD process, a short d_r distance leads to a porous flower-like morphology. This result suggests that WO_3 particles nucleate and grow homogenously before reaching the substrate. Our FESEM analysis suggests that d_r has a vital role in controlling the thickness and porosity of layers.

Moreover, when d_r remains constant, and the relative position of substrate changes, the thickness remains unaffected. It should also be noted that all the obtained films showed high adhesion to the substrate. Indeed, we have made many samples at distances closer to the nozzle that, despite their excellent porosity, suffer from sufficient adhesion, which showed high electrical resistance and excluded from this study. Therefore, the layer conditions of the reported samples are optimal for gas sensing applications.

3.3. Gas sensing characteristics

To increase the sensitivity to hydrogen gas, we deposited a thin Pd layer on the SF-FVD WO_3/Al_2O_3 samples. Then, sensing characteristics were explored by the time variation of the electrical resistance on the gas introduction (Fig. 4). The *n*-type nature of WO_3 is responsible for the electrical resistance decreased in the presence of hydrogen gas and increased in the presence of air. The sensing response, R, was defined in

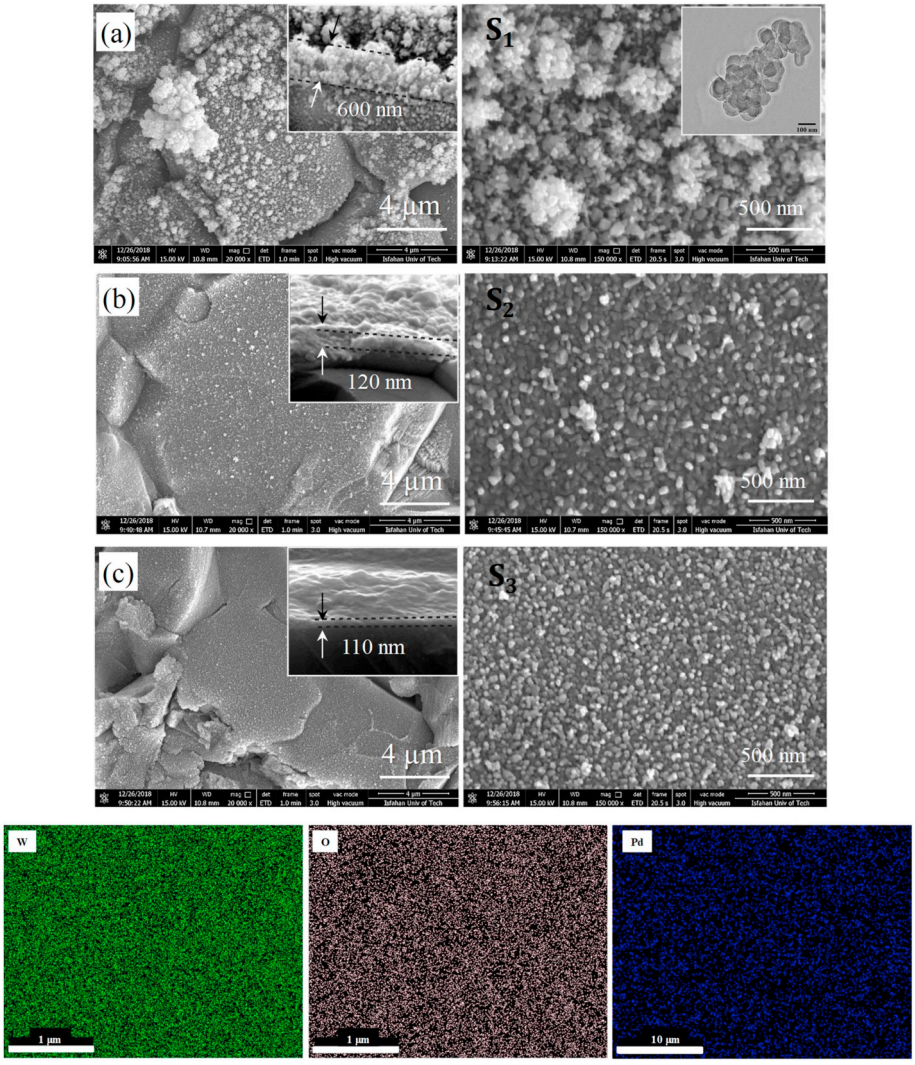

Fig. 3. Top view FESEM images of SF-FVD derived WO_3/Al_2O_3 films for S_1 (a), S_2 (b), and S_3 (c) at different magnifications. Insets show the cross-section images. A typical TEM image is shown for sample S_1. The bottom panel shows a typical EDS elemental map of Pd/WO_3 layers, indicating the presence of W, O, and Pd elements.

Eq. (1). For all the samples, S increases abruptly on hydrogen introduction but does not plateau. It drops slightly, which is less pronounced at lower gas concentrations. A thermodynamic equilibrium in the concentration of adsorbed H_2 molecules can be responsible for this drop [48]. Replacing the hydrogen with air returns S to the initial backgrounds, indicating a good reversibility behavior.

Fig. 5 shows the log-log plot of response to hydrogen gas of samples as a function of gas concentration. Each sample represents linear behavior almost at each working temperature, in agreement with the power-law behavior of the metal oxide gas sensors [49]. The sensor response was analyzed using the power law of gas sensors based on metal oxide semiconductors:

$$R = AC^{\beta} \tag{2}$$

where R is the sensor response, A is a pre-factor that depends on sensing component, and the working temperature, C is the gas concentrations, and β is the exponent factor that can have values of 0.5 or 1 depending on the charge state of surface oxygen atoms [50]. The obtained β values are summarized in Table .3. As can be seen, the values obtained are close to 1, suggesting that surface oxygen atoms are nearly in O^- states. For reducing gases like H_2, it has been known that they produce water in reaction with surface oxygen. When Pd/WO_3 grains are exposed to air, oxygen molecules existing in air atmosphere, chemisorb and get contact with the Pd clusters formed on WO_3 grains, and catalytically dissociated to form O atoms [51]:

$$O_2 \Leftrightarrow 2O_{atom} \tag{3}$$

The newly formed oxygen atoms can spillover from Pd catalyst to WO_3 surface. They trap free electrons from the conduction band of WO_3 semiconductor due to their high electron affinity and form O^- ions and remain on the surface

$$O_{atom} + e^-_{(fromWO3)} \Leftrightarrow O^- \tag{4}$$

This capturing leads to the development of a depletion layer on the surface and increases the potential barrier height between grains, followed by dropping the concentration of electrons and increasing the resistance and provides the baseline resistance. Accordingly, one can suggest the following reaction for hydrogen sensing mechanism in SF-FVD WO_3 films:

$$H_2(gas) + O^-(WO_3\ surface) \rightarrow H_2O + e^- \tag{5}$$

In addition, the adsorbed H_2 molecules are dissociated into H atoms

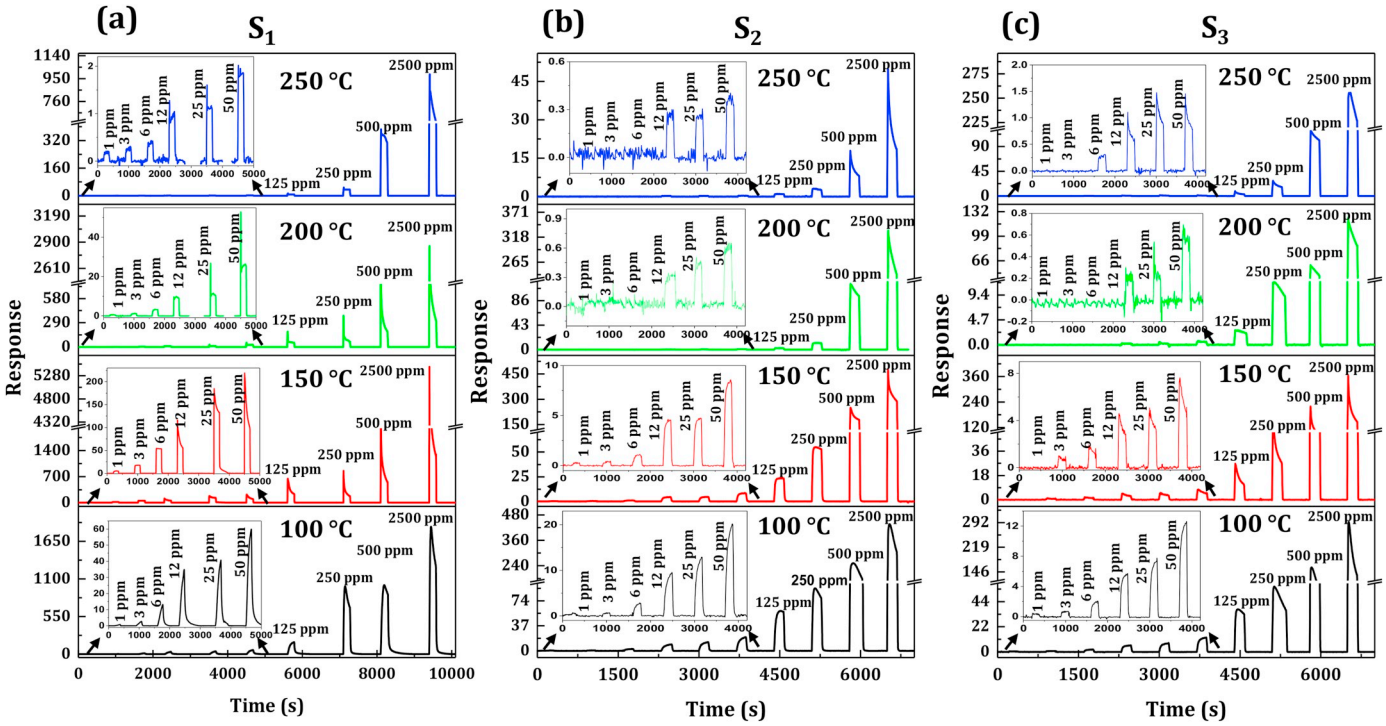

Fig. 4. Response of samples towards hydrogen gas at different concentrations and working temperatures.

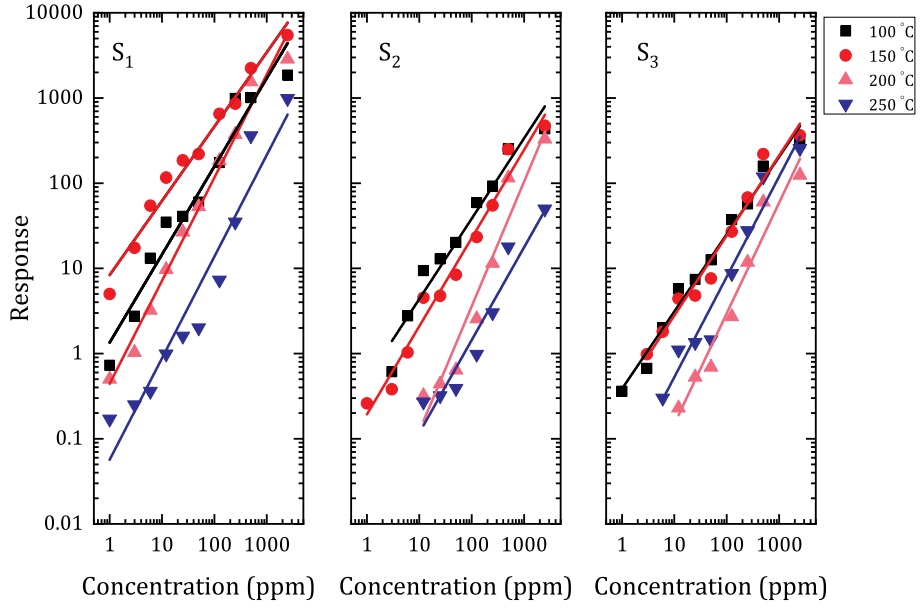

Fig. 5. Log-log plot of responses of samples as a function of hydrogen concentration for different working temperatures. (a) S_1, *(b) S_2, and (c) S_3.*

Table 3
Exponential coefficients, β, used to fit the power law in SF-FVD WO_3 sensors.

Sample	100 °C	150 °C	200 °C	250 °C
S_1	1.0	0.87	1.20	1.20
S_2	0.94	1.03	1.40	1.08
S_3	0.91	0.94	1.30	1.17

over the Pd layer then react with the oxygen of the WO_3 layer to produce tungsten oxide bronze ((H_xWO_3). This process also reduces W^{6+} to W^{5+}. As a result, oxygen vacancies release electron to the conduction band, leading to a decrease in the electrical resistance of the oxide layer [4,51–54]. It can be seen that the samples sensing response is better at temperatures of 100 and 150 °C. Particularly in sample S_1, the response is much higher at 100 °C than other existing data. Also, a decrease in the response value at higher temperatures, 200 and 250 °C, can be the result of an increase in the rate of gas desorption [4,51,55].

Fig. 6 shows the response and recovery times obtained from the dynamic response curves. Firstly, with increasing gas concentration, the response times reduce, and secondly, except at 100 °C, the response time is $<$ 50 s at the other temperatures. The recovery times are also near to 25 s at temperatures higher than 100 °C. Therefore, in terms of detection speed, the obtained SF-FVD WO_3 hydrogen sensors are sufficiently fast. In the case of the sample S_1, for which the rod-nozzle distance d_r is the smallest, the more open morphology of the WO_3 layer

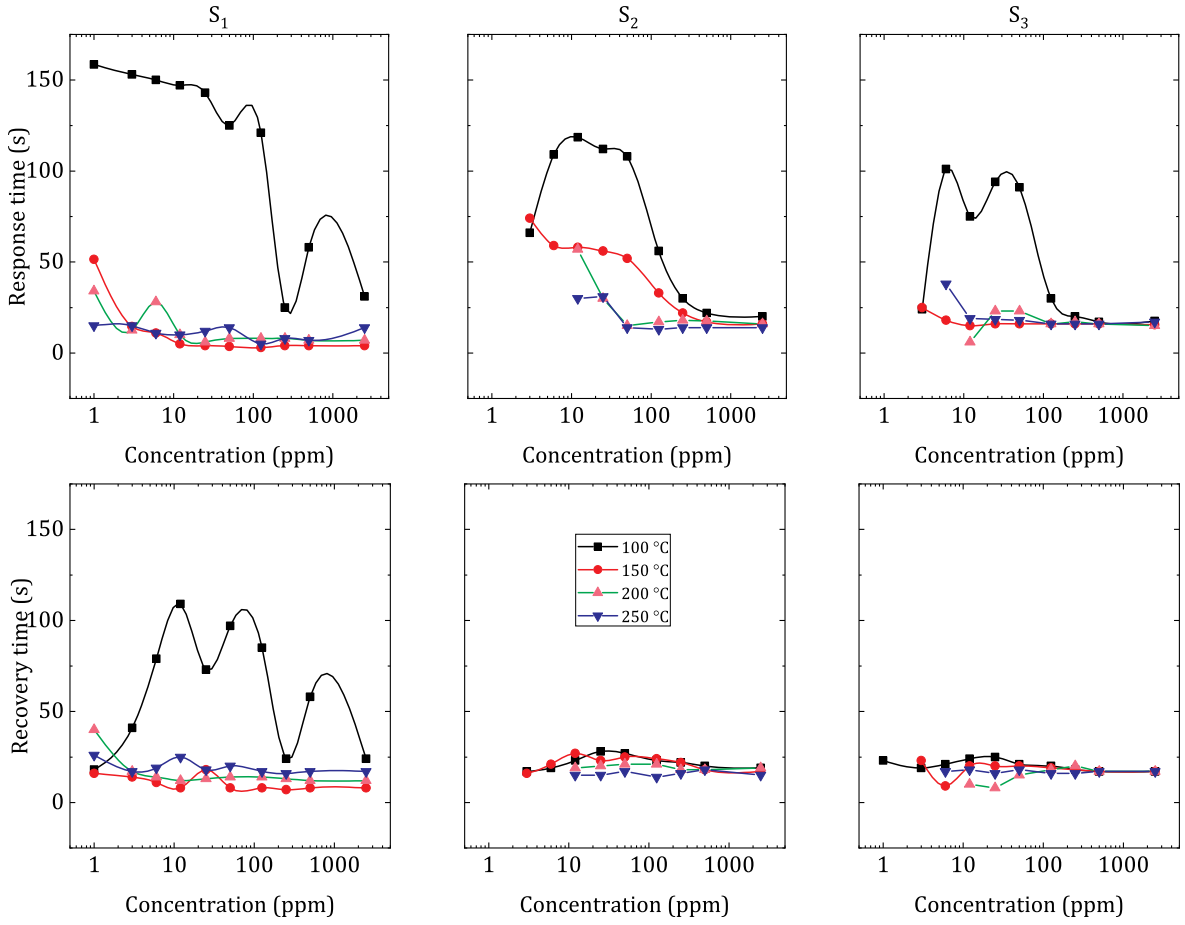

Fig. 6. Response time and recovery times of samples as a function of hydrogen concentration for different working temperatures.

(Fig. 2) can increase the gas diffusion rate into the layer pores and also enhance the surface adsorption. Therefore, the higher response values and better response/recovery times (Fig. 6) of S_1 are attributed to the layer morphology. Also, by increasing the working temperature, the diffusion and recombination rates are balanced for ions, leading to faster saturation velocity. Perhaps what the above results give us about the SF-FVD method is that, although the W rod and substrate displacements can affect the morphology and sensing characteristics, the samples have desirable sensing characteristics in all the conditions. One can conclude, therefore, that the SF-FVD method will provide devices of minimal tolerances in sensory properties in addition to being fast, mass-produced, and cost-effective.

Since sample S_1 showed better structural and sensing properties, it was used to investigate other hydrogen sensing features, including repeatability, stability, and selectivity. Fig. 7(a) shows the response and reusability of the WO_3 films in the concentration range of 75 to 1200 ppb. This graph shows two results, including the ability to reproduce well and the ability to measure hydrogen gas, even at ppb levels. Also, in the stability test shown in part (b), our product seems to have acceptable stability over 29 successive cycles with 12 ppm hydrogen gas. Therefore, the SF-FVD method can provide films with excellent reproducibility.

Fig. 7(c, d) shows the selectivity test results for sample S_1 at 150 °C towards 125 ppm H_2, CH_4 as reducing gases and NO_2 as an oxidative gas. It reveals a current response of about 440 nA towards hydrogen and a very weak response to CH_4 (14 nA). The current response is also negative for NO_2 because of its oxidative nature [56]. This negative response is 400 times smaller than the response to hydrogen gas. Therefore, the SF-FVD derived WO_3 based sensors are highly selective to hydrogen gas.

The selectivity of WO_3 films toward hydrogen has been vastly investigated elsewhere. Depending on the crystalline structure, working temperature, and type of the catalyst, WO_3 exhibit selectivity for different gases. For example, bare WO_3 with hexagonal structure has a very high selectivity for hydrogen sulfide [57]. The monoclinic structure requires high temperatures (> 300 °C) to detect gases such as volatile organic compounds (VOCs), CO, and NH_3. Below these temperatures, there is no significant response for these gases [58–60]. At lower temperatures (< 200 °C), NO_2 is better detected. The response of other reducing gases such as H_2 is negligible compared to NO_2 [56,61–64]. However, it has been shown that when the palladium is used as a catalyst, the tungsten oxide response to H_2 increases dramatically compared to other gases such as H_2S, CH_4, NH_3, CO, and VOC [2,65–68].

4. Conclusion

WO_3 hydrogen gas sensors are fabricated successfully by a solid-feed SF-FVD method. This method has the advantage of setup simplicity, which is low cost and fast. Fabricated sensors have a good ability to detect hydrogen at low concentrations (ppb level). By changing the deposition parameters, an optimum condition for sensor fabrication could be suggested. The selected hydrogen sensor has good stability during cycling and selectivity towards other reducing or oxidizing gases. Although SF-FVD parameters affect the gas sensing characteristics, the products are expected to have minimal tolerance in sensing of hydrogen gas, suitable for mass production of cost-effective hydrogen sensors.

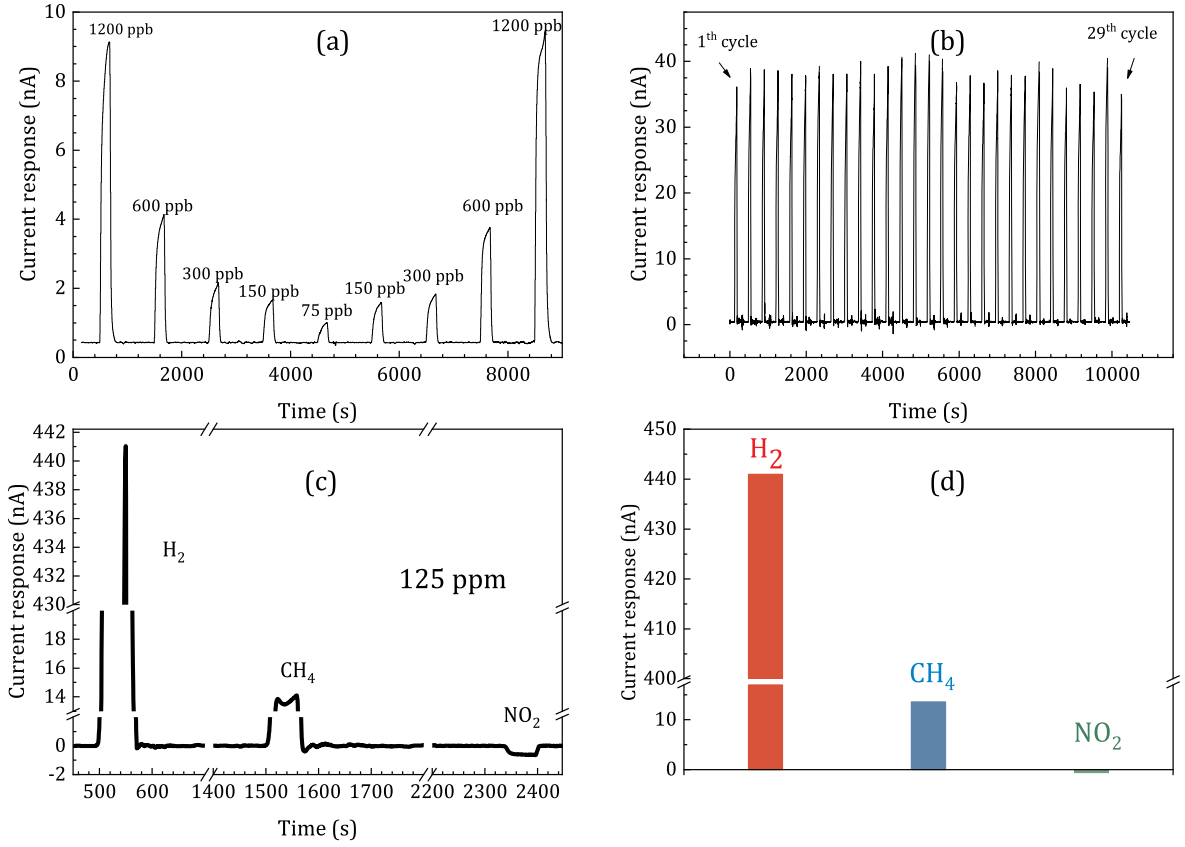

Fig. 7. (a) Reusability test of sample S_1 in the concentration range of 75–1200 ppb at 150 °C, (b) stability test of sample S_1 at 150 °C to 12 ppm hydrogen gas, (c, d) selectivity test for sample S_1 at 150 °C during exposure of deferent reducing and oxidizing gases.

Declaration of competing interest

None.

References

[1] M. Horprathum, T. Srichaiyaperk, B. Samransuksamer, A. Wisitsoraat, P. Eiamchai, S. Limwichean, C. Chananonnawathorn, K. Aiempanakit, N. Nuntawong, V. Patthanasettakul, C. Oros, S. Porntheeraphat, P. Songsiriritthigul, H. Nakajima, A. Tuantranont, P. Chindaudom, Ultrasensitive hydrogen sensor based on Pt-decorated WO3 nanorods prepared by glancing-angle dc magnetron sputtering, ACS Appl. Mater. Interfaces 6 (2014) 22051–22060, https://doi.org/10.1021/am505127g.

[2] S.J. Choi, S. Chattopadhyay, J.J. Kim, S.J. Kim, H.L. Tuller, G.C. Rutledge, I.D. Kim, Coaxial electrospinning of WO3 nanotubes functionalized with bio-inspired Pd catalysts and their superior hydrogen sensing performance, Nanoscale 8 (2016) 9159–9166, https://doi.org/10.1039/c5nr06611e.

[3] F.E. Annanouch, Z. Haddi, M. Ling, F. Di Maggio, S. Vallejos, T. Vilic, Y. Zhu, T. Shujah, P. Umek, C. Bittencourt, C. Blackman, E. Llobet, Aerosol-Assisted CVD-grown PdO nanoparticle-decorated tungsten oxide nanoneedles extremely sensitive and selective to hydrogen, ACS Appl. Mater. Interfaces 8 (2016) 10413–10421, https://doi.org/10.1021/acsami.6b00773.

[4] T. Samerjai, N. Tamaekong, C. Liewhiran, A. Wisitsoraat, A. Tuantranont, S. Phanichphant, Selectivity towards H2 gas by flame-made Pt-loaded WO 3 sensing films, Sensor. Actuator. B Chem. 157 (2011) 290–297, https://doi.org/10.1016/j.snb.2011.03.065.

[5] M. Amarnath, A. Heiner, K. Gurunathan, Surface bound nanostructures of ternary r-GO/Mn3O4/V2O5 system for room temperature selectivity of hydrogen gas, Ceram. Int. 46 (2020) 7336–7345, https://doi.org/10.1016/j.ceramint.2019.11.229.

[6] I.A. Nagornov, A.S. Mokrushin, E.P. Simonenko, N.P. Simonenko, P.Y. Gorobtsov, V.G. Sevastyanov, N.T. Kuznetsov, Zinc oxide obtained by the solvothermal method with high sensitivity and selectivity to nitrogen dioxide, Ceram. Int. 46 (2020) 7756–7766, https://doi.org/10.1016/j.ceramint.2019.11.279.

[7] K. Hu, F. Wang, H. Liu, Y. Li, W. Zeng, Enhanced hydrogen gas sensing properties of Pd-doped SnO2 nanofibres by Ar plasma treatment, Ceram. Int. 46 (2020) 1609–1614, https://doi.org/10.1016/j.ceramint.2019.09.132.

[8] A.A. Haidry, L. Xie, Z. Wang, Z. Li, Hydrogen sensing and adsorption kinetics on ordered mesoporous anatase TiO2 surface, Appl. Surf. Sci. 500 (2020) 144219, https://doi.org/10.1016/j.apsusc.2019.144219.

[9] H. Gu, Z. Wang, Y. Hu, Hydrogen gas sensors based on semiconductor oxide nanostructures, Sensors 12 (2012) 5517–5550, https://doi.org/10.3390/s120505517.

[10] G. Korotcenkov, V. Brinzari, I.A. Pronin, M.H. Ham, B.K. Cho, Metal oxides for application in conductometric gas sensors: how to choose? Solid State Phenom. 266 (2017) 187–195 https://doi.org/10.4028/www.scientific.net/SSP.266.187.

[11] S. Phanichphant, Semiconductor metal oxides as hydrogen gas sensors, Procedia Eng. 87 (2014) 795–802, https://doi.org/10.1016/j.proeng.2014.11.677.

[12] K. Inyawilert, A. Wisitsoraat, C. Liewhiran, A. Tuantranont, S. Phanichphant, H 2 gas sensor based on PdO x -doped in 2 O 3 nanoparticles synthesized by flame spray pyrolysis, Appl. Surf. Sci. 475 (2019) 191–203, https://doi.org/10.1016/j.apsusc.2018.12.274.

[13] G. Mattoni, B. De Jong, N. Manca, M. Tomellini, A.D. Caviglia, Single-crystal Pt-decorated WO3 ultrathin films: a platform for sub-ppm hydrogen sensing at room temperature, ACS Appl. Nano Mater. 1 (2018) 3446–3452, https://doi.org/10.1021/acsanm.8b00627.

[14] M. Zhao, J. Huang, C.W. Ong, Feasibility of H2 sensors composed of tungsten oxide nanocluster films, Int. J. Hydrogen Energy 38 (2013) 15559–15566, https://doi.org/10.1016/j.ijhydene.2013.09.069.

[15] D.H. Kim, J.S. Jang, W.T. Koo, S.J. Choi, H.J. Cho, M.H. Kim, S.J. Kim, I.D. Kim, Bioinspired cocatalysts decorated WO3 nanotube toward unparalleled hydrogen sulfide chemiresistor, ACS Sens. 3 (2018) 1164–1173, https://doi.org/10.1021/acssensors.8b00210.

[16] D. Abubakar, N.M. Ahmed, S. Mahmud, N.A. Algadri, Properties of NiO nanostructured growth using thermal dry oxidation of nickel metal thin film for hydrogen gas sensing at room temperature, Mater. Res. Express 4 (2017) 75009, https://doi.org/10.1088/2053-1591/aa76b1.

[17] Z. Li, S. Yan, Z. Wu, H. Li, J. Wang, W. Shen, Z. Wang, Y.Q. Fu, Hydrogen gas sensor based on mesoporous In2O3 with fast response/recovery and ppb level detection limit, Int. J. Hydrogen Energy 43 (2018) 22746–22755, https://doi.org/10.1016/j.ijhydene.2018.10.101.

[18] R. Ab Kadir, Z. Li, A.Z. Sadek, R. Abdul Rani, A.S. Zoolfakar, M.R. Field, J.Z. Ou, A.F. Chrimes, K. Kalantar-Zadeh, Electrospun granular hollow SnO2 nanofibers hydrogen gas sensors operating at low temperatures, J. Phys. Chem. C 118 (2014) 3129–3139, https://doi.org/10.1021/jp411552z.

[19] L. Liu, C. Liu, S. Li, L. Wang, H. Shan, X. Zhang, H. Guan, Z. Liu, Honeycombed SnO2 with ultra sensitive properties to H 2, Sensor. Actuator. B Chem. 177 (2013) 893–897, https://doi.org/10.1016/j.snb.2012.11.106.

[20] A. Hazra, S. Das, J. Kanungo, C.K. Sarkar, S. Basu, Studies on a resistive gas sensor based on sol-gel grown nanocrystalline p-TiO2 thin film for fast hydrogen detection, Sensor. Actuator. B Chem. 183 (2013) 87–95, https://doi.org/10.1016/j.snb.2013.03.113.

[21] O. Lupan, V. Postica, N. Ababii, M. Hoppe, V. Cretu, I. Tiginyanu, V. Sontea,

T. Pauporté, B. Viana, R. Adelung, Influence of CuO nanostructures morphology on hydrogen gas sensing performances, Microelectron. Eng. 164 (2016) 63–70, https://doi.org/10.1016/j.mee.2016.07.008.
[22] J. Hu, Y. Sun, Y. Xue, M. Zhang, P. Li, K. Lian, S. Zhuiykov, W. Zhang, Y. Chen, Highly sensitive and ultra-fast gas sensor based on CeO2-loaded In2O3 hollow spheres for ppb-level hydrogen detection, Sensor. Actuator. B Chem. 257 (2018) 124–135, https://doi.org/10.1016/j.snb.2017.10.139.
[23] K. Hassan, G.S. Chung, Catalytically activated quantum-size Pt/Pd bimetallic core–shell nanoparticles decorated on ZnO nanorod clusters for accelerated hydrogen gas detection, Sensor. Actuator. B Chem. 239 (2017) 824–833, https://doi.org/10.1016/j.snb.2016.08.084.
[24] J. Kukkola, M. Mohl, A.R. Leino, J. Mäklin, N. Halonen, A. Shchukarev, Z. Konya, H. Jantunen, K. Kordas, Room temperature hydrogen sensors based on metal decorated WO3 nanowires, Sensor. Actuator. B Chem. 186 (2013) 90–95, https://doi.org/10.1016/j.snb.2013.05.082.
[25] Y. Yao, F. Ji, M. Yin, X. Ren, Q. Ma, J. Yan, S.F. Liu, Ag nanoparticle-sensitized WO3 hollow nanosphere for localized surface plasmon enhanced gas sensors, ACS Appl. Mater. Interfaces 8 (2016) 18165–18172, https://doi.org/10.1021/acsami.6b04692.
[26] Y. Luo, C. Zhang, B. Zheng, X. Geng, M. Debliquy, Hydrogen sensors based on noble metal doped metal-oxide semiconductor: a review, Int. J. Hydrogen Energy 42 (2017) 20386–20397, https://doi.org/10.1016/j.ijhydene.2017.06.066.
[27] C. Zhang, A. Boudiba, M.G. Olivier, R. Snyders, M. Debliquy, Sensing properties of Pt/Pd activated tungsten oxide films grown by simultaneous radio-frequency sputtering to reducing gases, Sensor. Actuator. B Chem. 175 (2012) 53–59, https://doi.org/10.1016/j.snb.2011.11.060.
[28] G. Korotcenkov, V. Brinzari, B.K. Cho, Conductometric gas sensors based on metal oxides modified with gold nanoparticles: a review, Microchim. Acta. 183 (2016) 1033–1054, https://doi.org/10.1007/s00604-015-1741-z.
[29] C. Zhang, A. Boudiba, C. Navio, C. Bittencourt, M.G. Olivier, R. Snyders, M. Debliquy, Highly sensitive hydrogen sensors based on co-sputtered platinum-activated tungsten oxide films, Int. J. Hydrogen Energy 36 (2011) 1107–1114, https://doi.org/10.1016/j.ijhydene.2010.10.011.
[30] Y.S. Yoon, J.M. Im, D.W. Shin, Microstructure and electrical conductivity of NiO-YSZ nano-powder synthesized by aerosol flame deposition, Ceram. Int. 34 (2008) 873–876, https://doi.org/10.1016/j.ceramint.2007.09.039.
[31] J.M. Im, H.J. You, Y.S. Yoon, D.W. Shin, Synthesis of nano-crystalline Gd0.1Ce0.9O2-x for IT-SOFC by aerosol flame deposition, Ceram. Int. 34 (2008) 877–881, https://doi.org/10.1016/j.ceramint.2007.09.040.
[32] K. Bunpang, A. Wisitsoraat, A. Tuantranont, S. Phanichphant, C. Liewhiran, Effects of reduced graphene oxide loading on gas-sensing characteristics of flame-made Bi2WO6 nanoparticles, Appl. Surf. Sci. 496 (2019) 143613, https://doi.org/10.1016/j.apsusc.2019.143613.
[33] H.H. Nersisyan, J.H. Lee, J.R. Ding, K.S. Kim, K.V. Manukyan, A.S. Mukasyan, Combustion synthesis of zero-, one-, two- and three-dimensional nanostructures: current trends and future perspectives, Prog. Energy Combust. Sci. 63 (2017) 79–118, https://doi.org/10.1016/j.pecs.2017.07.002.
[34] J.A. Kemmler, S. Pokhrel, L. Mädler, U. Weimar, N. Barsan, Flame spray pyrolysis for sensing at the nanoscale, Nanotechnology 24 (2013), https://doi.org/10.1088/0957-4484/24/44/442001.
[35] T. Samerjai, N. Tamaekong, K. Wetchakun, V. Kruefu, C. Liewhiran, C. Siriwong, A. Wisitsoraat, S. Phanichphat, Flame-spray-made metal-loaded semiconducting metal oxides thick films for flammable gas sensing, Sensor. Actuator. B Chem. 171–172 (2012) 43–61, https://doi.org/10.1016/j.snb.2012.05.052.
[36] L. Cai, P.M. Rao, Y. Feng, X. Zheng, Flame synthesis of 1-D complex metal oxide nanomaterials, Proc. Combust. Inst. 34 (2013) 2229–2236, https://doi.org/10.1016/j.proci.2012.05.004.
[37] W. Merchan-Merchan, A.V. Saveliev, W.C. Jimenez, Solid support flame synthesis of 1-D and 3-D tungsten-oxide nanostructures, Proc. Combust. Inst. 33 (2011) 1899–1908, https://doi.org/10.1016/j.proci.2010.06.122.
[38] S.H. Yoon, K.S. Kim, Control of 1-dimensionally structured tungsten oxide thin films by precursor feed rate modulation in flame vapor deposition, J. Ind. Eng. Chem. 73 (2019) 52–57, https://doi.org/10.1016/j.jiec.2019.01.013.
[39] J.R. Ding, K.S. Kim, Rapid growth of vertically aligned tungsten oxide nanostructures by flame vapor deposition process, Chem. Eng. J. 300 (2016) 47–53, https://doi.org/10.1016/j.cej.2016.04.106.
[40] J.R. Ding, S.H. Yoon, W. Shi, K.S. Kim, Nanowire-based branched nanotrees prepared by flame vapor deposition system incorporated with double wire feeders, AIChE J. 65 (2019) 1138–1143, https://doi.org/10.1002/aic.16527.
[41] P.M. Rao, X. Zheng, Flame synthesis of tungsten oxide nanostructures on diverse substrates, Proc. Combust. Inst. 33 (2011) 1891–1898, https://doi.org/10.1016/j.proci.2010.06.071.
[42] Z. Qiao, Z. Wang, C. Zhang, S. Yuan, Y. Zhu, J. Wang, PVAm–PIP/PS composite membrane with high performance for CO_2/N_2 separation, AIChE J. 59 (2012) 215–228, https://doi.org/10.1002/aic.
[43] P.M. Rao, I.S. Cho, X. Zheng, Flame synthesis of WO3 nanotubes and nanowires for efficient photoelectrochemical water-splitting, Proc. Combust. Inst. 34 (2013) 2187–2195, https://doi.org/10.1016/j.proci.2012.06.122.
[44] J.R. Ding, K.S. Kim, Flame synthesized single crystal nanocolumn-structured wo3 thin films for photoelectrochemical water splitting, J. Nanosci. Nanotechnol. 16 (2016) 1578–1582, https://doi.org/10.1166/jnn.2016.11937.
[45] A.R. Shafieyan, M. Ranjbar, P. Kameli, Localized surface plasmon resonance H2 detection by MoO3 colloidal nanoparticles fabricated by the flame synthesis method, Int. J. Hydrogen Energy 44 (2019) 18628–18638, https://doi.org/10.1016/j.ijhydene.2019.05.171.
[46] Y.M. Hunge, M.A. Mahadik, A.V. Moholkar, C.H. Bhosale, Photoelectrocatalytic degradation of phthalic acid using spray deposited stratified WO 3/ZnO thin films under sunlight illumination, Appl. Surf. Sci. 420 (2017) 764–772, https://doi.org/10.1016/j.apsusc.2017.05.221.
[47] V.V. Zuev, S.N. Grigoriev, R.I. Romanov, V.Y. Fominski, M.A. Volosova, M.V. Demin, Comparative studies of monoclinic and orthorhombic WO3 films used for hydrogen sensor fabrication on SiC crystal, J. Phys. Conf. Ser. 747 (2016) 12050, https://doi.org/10.1088/1742-6596/747/1/012050.
[48] G. Hussain, M. Ge, C. Zhao, D.S. Silvester, Fast responding hydrogen gas sensors using platinum nanoparticle modified microchannels and ionic liquids, Anal. Chim. Acta 1072 (2019) 35–45, https://doi.org/10.1016/j.aca.2019.04.042.
[49] V.B. Kamble, A.M. Umarji, Achieving selectivity from the synergistic effect of Cr and Pt activated SnO2 thin film gas sensors, Sensor. Actuator. B Chem. 236 (2016) 208–217, https://doi.org/10.1016/j.snb.2016.05.119.
[50] B. Urasinska-Wojcik, T.A. Vincent, J.W. Gardner, H2S sensing properties of WO3 based gas sensor, Procedia Eng., 2016, pp. 255–258, https://doi.org/10.1016/j.proeng.2016.11.181.
[51] A. Boudiba, P. Roussel, C. Zhang, M.G. Olivier, R. Snyders, M. Debliquy, Sensing mechanism of hydrogen sensors based on palladium-loaded tungsten oxide (Pd-WO3), Sensor. Actuator. B Chem. 187 (2013) 84–93, https://doi.org/10.1016/j.snb.2012.09.063.
[52] F.H. Tian, C. Gong, Y. Peng, X. Xue, H2 sensing mechanism under different oxygen concentration on the hexagonal WO3 (001) surface: a density functional theory study, Sensor. Actuator. B Chem. 244 (2017) 655–663, https://doi.org/10.1016/j.snb.2016.12.035.
[53] S.S. Kalanur, I.H. Yoo, Y.A. Lee, H. Seo, Green deposition of Pd nanoparticles on WO3 for optical, electronic and gasochromic hydrogen sensing applications, Sensor. Actuator. B Chem. 221 (2015) 411–417, https://doi.org/10.1016/j.snb.2015.06.086.
[54] Y. Wang, B. Liu, S. Xiao, H. Li, L. Wang, D. Cai, D. Wang, Y. Liu, Q. Li, T. Wang, High performance and negative temperature coefficient of low temperature hydrogen gas sensors using palladium decorated tungsten oxide, J. Mater. Chem. A. 3 (2015) 1317–1324, https://doi.org/10.1039/c4ta05229c.
[55] M. Zhao, J.X. Huang, C.W. Ong, Diffusion-controlled H2 sensors composed of Pd-coated highly porous WO3 nanocluster films, Sensor. Actuator. B Chem. 191 (2014) 711–718, https://doi.org/10.1016/j.snb.2013.09.116.
[56] C. Wang, M. Ding, X. Kou, L. Guo, C. Feng, X. Li, H. Zhang, P. Sun, Y. Sun, G. Lu, Detection of nitrogen dioxide down to ppb levels using flower-like tungsten oxide nanostructures under different annealing temperatures, J. Colloid Interface Sci. 483 (2016) 314–320, https://doi.org/10.1016/j.jcis.2016.08.050.
[57] I.M. Szilágyi, S. Saukko, J. Mizsei, A.L. Tóth, J. Madarász, G. Pokol, Gas sensing selectivity of hexagonal and monoclinic WO3 to H2S, Solid State Sci. 12 (2010) 1857–1860, https://doi.org/10.1016/j.solidstatesciences.2010.01.019.
[58] S. Wei, Y. Xing, Y. Li, Y. Zhao, W. Du, M. Zhou, Preparation and gas sensing properties of flower-like WO3 hierarchical architecture, Vacuum 129 (2016) 13–19, https://doi.org/10.1016/j.vacuum.2016.04.010.
[59] S. Park, H. Kim, C. Jin, S.-W. Choi, S.S. Kim, C. Lee, Enhanced CO gas sensing properties of Pt-functionalized WO3 nanorods, Thermochim. Acta 542 (2012) 69–73, https://doi.org/10.1016/j.tca.2011.12.002.
[60] P. Van Tong, N.D. Hoa, N. Van Duy, D.T.T. Le, N. Van Hieu, Enhancement of gas-sensing characteristics of hydrothermally synthesized WO3 nanorods by surface decoration with Pd nanoparticles, Sensor. Actuator. B Chem. 223 (2016) 453–460, https://doi.org/10.1016/j.snb.2015.09.108.
[61] Y.-S. Shim, L. Zhang, D.H. Kim, Y.H. Kim, Y.R. Choi, S.H. Nahm, C.-Y. Kang, W. Lee, H.W. Jang, Highly sensitive and selective H2 and NO2 gas sensors based on surface-decorated WO3 nanoigloos, Sensor. Actuator. B Chem. 198 (2014) 294–301, https://doi.org/10.1016/j.snb.2014.03.073.
[62] T.H. Kim, A. Hasani, L. Van Quyet, Y. Kim, S.Y. Park, M.G. Lee, W. Sohn, T.P. Nguyen, K.S. Choi, S.Y. Kim, H.W. Jang, NO2 sensing properties of porous Au-incorporated tungsten oxide thin films prepared by solution process, Sensor. Actuator. B Chem. 286 (2019) 512–520, https://doi.org/10.1016/j.snb.2019.02.009.
[63] R. Jain, Y. Lei, R. Maric, Ultra-low NO2 detection by gamma WO3 synthesized by reactive spray deposition technology, Sensor. Actuator. B Chem. 236 (2016) 163–172, https://doi.org/10.1016/j.snb.2016.05.134.
[64] C. Wang, X. Li, C. Feng, Y. Sun, G. Lu, Nanosheets assembled hierarchical flower-like WO3 nanostructures: synthesis, characterization, and their gas sensing properties, Sensor. Actuator. B Chem. 210 (2015) 75–81, https://doi.org/10.1016/j.snb.2014.12.020.
[65] F.E. Annanouch, Z. Haddi, M. Ling, F. Di Maggio, S. Vallejos, T. Vilic, Y. Zhu, T. Shujah, P. Umek, C. Bittencourt, C. Blackman, E. Llobet, Aerosol-Assisted CVD-grown PdO nanoparticle-decorated tungsten oxide nanoneedles extremely sensitive and selective to hydrogen, ACS Appl. Mater. Interfaces 8 (2016) 10413–10421, https://doi.org/10.1021/acsami.6b00773.
[66] T. Samerjai, N. Tamaekong, C. Liewhiran, A. Wisitsoraat, A. Tuantranont, S. Phanichphant, Selectivity towards H2 gas by flame-made Pt-loaded WO3 sensing films, Sensor. Actuator. B Chem. 157 (2011) 290–297, https://doi.org/10.1016/j.snb.2011.03.065.
[67] X. Geng, Y. Luo, B. Zheng, C. Zhang, Photon assisted room-temperature hydrogen sensors using PdO loaded WO3 nanohybrids, Int. J. Hydrogen Energy 42 (2017) 6425–6434, https://doi.org/10.1016/j.ijhydene.2016.12.117.
[68] S. Kabcum, D. Channei, A. Tuantranont, A. Wisitsoraat, C. Liewhiran, S. Phanichphant, Ultra-responsive hydrogen gas sensors based on PdO nanoparticle-decorated WO3 nanorods synthesized by precipitation and impregnation methods, Sensor. Actuator. B Chem. 226 (2016) 76–89, https://doi.org/10.1016/j.snb.2015.11.120.